1 **Performance of the Global Forecast System's Medium-Range**
2 **Precipitation Forecasts in the Niger River Basin**

3 Haowen Yue[1], Mekonnen Gebremichael[1], and Vahid Nourani[2]

4 [1] Department of Civil and Environmental Engineering, University of California, Los Angeles, CA 90095-1593
5 [2] Faculty of Civil Engineering, University of Tabriz, Tabriz, Iran
6

7

8 *Correspondence to*: Haowen Yue (yuehaowen@g.ucla.edu)

9

Hydrology and
Earth System
Sciences
Discussions

10   **Abstract.** Weather forecast information has the potential to improve water resources management, energy, and

11   agriculture. This study evaluates the accuracy of medium-range (1 – 15 day) precipitation forecasts from the Global

12   Forecast System (GFS) over watersheds of eight major dams in the Niger river basin. The Niger basin lies in three

13   latitudinal/climatic sub-regions: Sahel (latitude > 12°N) with annual rainfall of rainfall 400–600 mm, Savannah

14   (latitude 8°–12°N) with annual rainfall of 900-1200 mm, and Guinea Coast (latitude 4°–8°N) with annual rainfall of

15   1500-2000 mm. The GFS forecast tends to overestimate rainfall in the Guinea Coast and western parts of the

16   Savannah, but estimates well in the Sahel. The overall performance of daily GFS forecast was found to be satisfactory

17   for two watersheds, namely, Kainji (the largest watershed in the basin, predominantly located in the Sahel), and

18   Markala (the second largest watershed, located partly in the Sahel and partly in the Savannah). However, the

19   performance of daily GFS forecast was found to be unsatisfactory in the remaining six watersheds, with GFS forecasts

20   characterized by large random errors, high false alarm, high overestimation bias of low rain rates, and large

21   underestimation bias of heavy rain rates. The GFS forecast accuracy decreases with increasing lead time. The accuracy

22   of GFS forecasts could be improved by applying post-processing techniques involving near-real time satellite rainfall

23   products.

24

25

26

Hydrology and
Earth System
Sciences
Open Access
Discussions
EGU

1. Introduction

Global climate forecasts, with lead times ranging from hours to several months, are becoming increasingly available (Saha et al. 2011; Abdalla et al. 2013; NCEP 2015; JMA 2019). Significant societal benefit could be realized from research to reduce common barriers in climate forecast utilization blocking the path to improving water resources management, energy, and agriculture. One such a barrier is the lack of understanding of climate forecast accuracy in different regions of the world. This focus is timely given the recent advances in numerical atmospheric models, and in the wealth of new observing capabilities including satellite remote sensing. These combined models and observational datasets provide opportunity for researchers to quantify the accuracy of climate forecasts.

The Niger River is the principal river of West Africa, and is shared among nine riparian countries (Fig. 1): Benin, Burkina Faso, Cameroon, Chad, Guinea, Ivory Coast, Mali, Nige and Nigeria. The basin is facing multiple pressures from increasing population, water abstraction for irrigation, and risk of extreme hydrological events due to climate change (Sylla et al. 2018). A number of hydropower dams exist in the region, and additional dam projects are envisaged in order to alleviate chronic power shortages in the countries of the Niger basin. Optimal management of water resources is key to maximizing benefits, such as hydropower generation, and minimize disasters, such as flooding. Climate forecast information has the potential to improve water resources management, energy, and agriculture (e.g., Patt et al. 2007; Breuer et al. 2010; Mase and Prokopy 2014; Pandya et al. 2015; Koppa et al. 2019; Alexander et al. 2021). For example, in a recent study, Koppa et al (2019) showed that the use of seasonal precipitation forecasts in reservoir planning of Omo Gibe dam in Ethiopia can increase annual hydropower generation by around 40%.

Several studies have investigated the accuracy of seasonal forecasts in West Africa (e.g., Bliefernicht et al. 2019; Pirret et al. 2020). Seasonal forecasts are important for water resource planning, while medium-range (1-day to 15-day) forecasts are important for operational decisions, such as reservoir operations. The availability of medium-range global climate forecasts has grown in recent years. Examples of such forecast products include Global Forecast System (GFS; NCEP 2015), NCEP climate forecast system (NSF CFS, Saha et al. 2014), European Centre for Medium-Range Weather Forecasts (ECMWF; Abdalla et al. 2013), and Global Spectral Model (GSM; JMA 2019). For these precipitation forecasts to be effectively used in applications, their accuracy must be known, which is usually performed

55   through comparison of precipitation forecasts to observations (e.g., Tian et al. 2017; Yuan et al. 2014). Yet, to the best

56   of our knowledge, there has not been any medium-range forecast evaluation study in the Niger River Basin. Recent

57   advances in satellite rainfall products, particularly following the Global Satellite Measurement satellite mission (GPM;

58   Hou et al. 2014), provide opportunity to serve as independent, and relatively more accurate, references to evaluate

59   climate forecasts.

60

61   Many studies have conducted to evaluate the accuracy of the satellite rainfall estimates in West Africa. Dezfuli et al.

62   (2017a) evaluated the performance of IMERG Final (version 4) in comparison with two, high-resolution, experimental

63   rain gauge station data provided by the Trans-African Hydro-Meteorological Observatory (TAHMO; van de Giesen

64   et al. 2014), and reported the capability of IMERG Final to represent well the diurnal cycle of rainfall. Using the same

65   dataset, Dezfuli et al. (2017b) showed that IMERG Final is able to capture the propagation of large Mesoscale

66   Convective Systems (MCSs), a significant advantage over its predecessor's (TMPA) 3-hourly temporal resolution,

67   which misses the time evolution of most of these systems. Gossett et al. (2018) evaluated the performance of a number

68   of satellite rainfall products (focusing only on versions that do not include rain gauge data) by comparison with rain

69   gauge station networks in Benin and Niger, and reported that the satellite products (especially IMERG Early) exhibit

70   high performance in Niger but relatively lower performance in Benin. Satge et al. (2020) evaluated the accuracy of a

71   number of gridded precipitation datasets over West Africa through comparison against rain gauge station data, and

72   reported that CHIRPS and TMPA (the predecessor to IMERG) provided reliable estimates at both daily and monthly

73   timescales, while the remaining satellite products considered (CMORPH, PERSIANN, GSMaP, ARC, and TAMSAT)

74   and all atmospheric reanalysis products considered (MERRA and JRA) were deemed unreliable. Furthermore, they

75   found out that satellite products that incorporated rain gauge information outperformed satellite-only products.

76   Maranan et al. (2020) compared IMERG Fsatellite gauged) products against experimental rain gauge station data in

77   the moist forest region of Ghana, West Africa, and showed that IMERG Final datasets are able to capture monthly

78   rainfall with a correlation coefficient close to unity.

79

80   The GFS outstands itself by providing free medium range forecasts at a relatively high temporal and spatial resolution.

81   Besides, the GFS is being constantly improved by the developers, showing promising future applications. The

82   advantages of GFS motivate this study to evaluate the accuracy of medium-range precipitation forecasts derived from

83 the Global Forecast System (GFS) for the major reservoir dams of the Niger basin through comparison against

84 satellite-based rainfall observational datasets known as NASA's Integrated Multi-satellitE Retrievals (IMERG) "Final

85 Run" (IMERG Final). The main questions addressed in this study are as follows. First, how does the accuracy of GFS

86 forecast vary across different reservoir dams in the same basin? Second, how does the accuracy vary with lead time

87 in the range 1- to 15-day? Third, what is the effect of spatial averaging (from 0.25° all the way to basin-scale) and

88 temporal aggregation (from 1-day to 15-day) on the forecast accuracy? Fourth, how does the accuracy of GFS forecast

89 compare with the accuracy of satellite-only rainfall products that are available in near-real-time, as the latter may have

90 the potential to calibrate and improve the accuracy of GFS?

91

92 **2.   Data and Methodology**

93 **2.1 Global Forecast System (GFS) Medium-Range Precipitation Forecasts**

94 The Global Forecast System (GFS) most-recent version (version 15) precipitation forecasts, that are available since

95 12 June 2019 are used in this study. The GFS forecasts are available at a spatial resolution of 0.25° by 0.25°, a temporal

96 resolution of hourly for the first 120 hours (i.e. 5 days) and 3-hourly for days 5-16, and lead times ranging from 1 hour

97 up to 16 days. The GFS forecasts are obtained from National Center for Atmospheric Research (NCAR) Research

98 Data Archive (RDA) GFS Historical Archive (NCEP 2015; https://rda.ucar.edu/datasets/ds084.1/; last accessed: April

99 2021).

100

101 The GFS is a global numerical weather prediction system run by the U.S. National Weather Service (NWS). The GFS

102 is run four times a day (UTC00, UTC06, UTC12 and UTC18). The latest version (version 15) of GFS model utilizes

103 the Finite Volume Cubed Sphere (FV3) model as the core physical model, which is developed by the Geophysical

104 Fluid Dynamics Laboratory (GFDL) (Putman and Lin, 2007). Key model schemes include: (1) the Rapid Radiative

105 Transfer Method for GCMs (RRTMG) scheme for shortwave/longwave radiation (Mlawer et al. 1997; Iacono et al.

106 2000; Clough et al. 2005), (2) the Hybrid eddy-diffusivity mass-flus (EDMF) scheme for Planetary Boundary Layer

107 (PBL) (NCEP, 2019a), (3) the Noah Land Surface Model (LSM) scheme for land surface option (Chen et al. 1997),

108 (4) the Simplified Arakawa-Schubert (SAS) deep convection for cumulus parameterization (Arakawa et al. 1974;

109 Grell 1993), and (5) an advanced GFDL microphysics scheme for microphysics (NCEP, 2019b).

110

111 **2.2 IMERG Final Satellite Precipitation Products**

112 IMERG Final rainfall products are used in this study as reference to evaluate the performance of GFS precipitation

113 forecasts. IMERG Final combines all available microwave precipitation estimates, microwave-calibrated infrared

114 estimates, and rain gauge data to provide rainfall estimates at very high resolution (30-minute, 0.10°) (Hou et al., 2014;

115 Huffman et al., 2018). The IMERG products are categorized into three types, namely early run, late run, and final run.

116 It is only the final run or "final" version that incorporates rain gauge data. The data latency of IMERG Final is about

117 3.5 months. Details of IMERG algorithm developed by NASA are available at Huffman et al (2019a, 2019b). The

118 latest version (V6B) of IMERG datasets have been obtained from the NASA's Earth Data Goddard Earth Sciences

119 Data and Information Services Center (GESDISC) web portal (https://disc.gsfc.nasa.gov/; last accessed: April 2021).

120

121 **2.3 Other Satellite Precipitation Products**

122 In order to put the GFS forecast performance into perspective and also consider the effect of reference rainfall

123 product choice, we evaluated other state-of-the-art satellite rainfall products:

124 • IMERG Early provides un-calibrated IMERG rainfall fields, which do not include correction from rain gauges.

125   The data latency of IMERG Early is near-real-time, about 4 hours. The latest version (V6B) of IMERG Early

126   datasets have been obtained from the NASA's GESDISC web portal (https://disc.gsfc.nasa.gov/; last accessed:

127   April 2021).

128 • The Climate Hazard's group Infrared Precipitation (CHIRP) and with Stations (CHIRPS) dataset is derived

129   primarily from thermal infrared data using the cold cloud duration (CCD) approach, calibrated using TRMM

130   Multi-satellite Precipitation analysis (TMPA 3B42 v7; Huffman et al. 2007) precipitation datasets by local

131   regression, and include rain gauge station data from multiple sources (regional and national meteorological

132   services). CHIRPS data are available at a spatial resolution of 0.05° and a temporal resolution of 1-day, with a

133   data latency period of about 3 weeks. Details of CHIRPS algorithm are available at Funk et al. (2015). CHIRPS

134   rainfall products are obtained from the CHIRPS webpage (https://www.chc.ucsb.edu/data; version 2.0 accessed

135   in April 2021).

136 • IMERG Early Cal – provides climatologically bias-corrected IMERG rainfall fields. We created this product by

137   bias (multiplicative bias) correction of IMERG Early on the basis of IMERG Final on a pixel-by-pixel (i.e. 0.10°)

138   and monthly rainfall accumulation timescale.

139

140   **2.4 Evaluation**

141   The Niger river, with a drainage basin of 2,117,700 Sq. Km in area, is the third longest river in Africa. The source of

142   the main river is in the Guinea Highlands, and runs through Mali, Niger, on the border with Benin and then through

143   Nigeria, discharging through a massive delta, known as the Niger Delta (the world's third largest wetland), into the

144   Atlantic Ocean. West African rainfall regimes follow the seasonal migration of the intertropical the Intertropical

145   Convergence Zone, which brings rainfall primarily in the summer season (Animashaun et al. 2020; Sorí et al. 2017).

146   Climatologically, the Niger basin lies in three latitudinal sub-regions (Akinsanola et al. 2015, 2017): (1) the Guinea

147   coast (latitude 4°–8°N), which borders the tropical Atlantic Ocean in the south; (2) the Savannah (latitude 8°–12°N),

148   an intermediate sub-region; and (3) the Sahel (latitude > 12°N) to the north. The Guinea coast experiences a

149   bimodal rainfall regime that is centered in the summer monsoon period of June–September, with August being the

150   period of a short dry season, while the Savannah and Sahel sub-regions experience a unimodal rainfall regime, with

151   maximum rainfall occurring in August (Akinsanola and Zhou, 2018). The ranges of annual rainfall amount are 400–

152   600 mm in the Sahel, 900–1200 mm in the Savannah; and 1500–2000 mm in the Guinea coast (Akinsanola et al.,

153   2017).

154

155   The Niger basin is home to eight major reservoir dams (see Table 1 and Fig. 1): (1) Selingue Dam in Mali: a primarily

156   hydropower dam, (2) Markala Dam in Mali: a primarily irrigation dam, serving about 75,000 ha of farmland, (3)

157   Goronyo Dam in Nigeria: primary purpose is for flood control, provision of downstream water supply and the release

158   of water for irrigation in the dry season, (4) Bakolori Dam in Nigeria: a primarily irrigation dam with a command area

159   of about 23,000 ha, (5) Kainji Dam in Nigeria: the largest Dam on the Niger supplying power for most towns in

160   Nigeria, (6) Jebba Dam in Nigeria: a primarily hydropower dam, (7) Dadin Kowa Dam: a multi-purpose dam for

161   water supply, electricity and irrigation, (8) Lagdo Dam in Cameroon: provides electricity to the northern part of the

162   country and allow the irrigation of 15,000 hectares of crops downstream. The watersheds of the dams are primarily

163   either in the Savanna (Selingue, Markala, Jebba, Dadin Kowa, an Lagdo), or in the Sahel (Goronyo, Kainji), or partly

164   in both (Bakolori). The watershed sizes vary over a large range, from 4,887 m^2 for Markala Dam to 1,464,092 for

165   Kainji Dam. The average elevations of the watersheds are close to each other at 500 ± 50 m.a.s.l.

166

167

168   Table 1. Selected dams for this study, and their watershed characteristics

169

Dam	Country	Operational since	Capacity (million m³)	Power (MW)	Primary Purpose			Area of Drainage Basin (km²)	Elevation of Drainage Basin (m)
					Irrigation and Water Supply	Flood Control	Hydroelectricity		
Selingue	Mali	1982	2170	44			x	32685	473
Markala	Mali	1947	175		x			102882	442
Goronyo	Nigeria	1983	942		x	X		31547	446
Bakolori	Nigeria	1978	450		x			4887	519
Kainji	Nigeria	1968	15000	960			x	1464092	406
Jebba	Nigeria	1984	3600	540			x	40268	308
Dadin Kowa	Nigeria	1988	2855	35	x		x	32936	535
Lagdo	Cameroon	1983	7800	72		x	x	31352	452

170
171
172

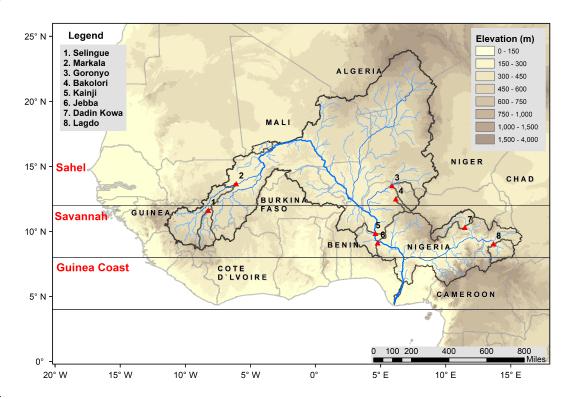173

174

175

176

177

178

179

180

181

182

183

Figure 1. The Niger River Basin, and locations of major reservoir dams in the basin: (1) Selingue, (2) Markala, (3) Goronyo, (4) Bakolori, (5) Kainji, (6) Jebba, (7) Dadin Kowa, and (8) Lagdo.

184

185

186

187

188

189

190

191

192

193

194

195

196

Hydrology and
Earth System
Sciences
Discussions

Open Access
EGU

197   In order to make the results of this study meaningful to reservoir managers, the Niger basin was divided into

198   watersheds according to the locations of the dam reservoirs (see Fig. 1). Then the sub-basin of each dam was defined

199   as the drainage between the dam itself and the previous dam. For example, the drainage basin of the Markala Dam

200   does not include the drainage basin of the Selingue Dam.

201

202   For evaluation metrics, we used the Kling-Gupta Efficiency (KGE; Gupta et al. 2009) and its components: Bias Ratio

203   (BR), correlation (R), and variability ratio (γ). *KGE* measures the goodness-of-fit between estimates of precipitation

204   forecasts and reference observations as:

205   $$KGE = 1 - \sqrt{(R-1)^2 + (BR-1)^2 + (\gamma-1)^2},$$

206   $$BR = \frac{\mu_f}{\mu_o},$$

207   $$\gamma = \frac{CV_f}{CV_o},$$

208   where R is the linear correlation coefficient between forecasted and observed precipitation, BR is the bias ratio, γ is

209   the variability ratio, μ is the mean precipitation, CV is the coefficient if variation, and the indices *f* and *o* represent

210   forecasted and observed precipitation values, respectively. KGE values range from -∞ to 1, with values closer to 1

211   indicating better model performance. Kling et al. (2012) suggested the following classifications: "Good" (KGE ≥

212   0.75), "Intermediate" (0.75 ≥ KGE ≥ 0.5), "Poor" (0.5 ≥ KGE > 0), and "Very poor" (KGE ≤ 0). The *BR* values

213   greater than 1 indicate a positive bias whereby forecasts overestimate precipitation relative to the observed data,

214   while values less than 1 represent an underestimation. *The γ* values greater than 1 indicate that the variability in the

215   forecast time series is higher than that observed, and values less than 1 show the opposite effect. The *R* measures the

216   strength and direction of the linear relationship between the forecast and observed values. The correlation values of

217   0.6 or more are considered to be skillful (e.g., Alfieri et al. 2013). In addition, the root mean-square-error normalized

218   by reference precipitation mean (NRMSE) was also used to measure the efficiency of the products.

219

220

221

222

223 ## 3. Results and Discussion

224 ### 3.1 Annual Spatial Variability and Seasonal Characteristics

225 The spatial map of annual (15 June 2019 – 15 June 2020) rainfall from the various rainfall products is given in Figure

226 2. According to the reference rainfall product (i.e. IMERG Final), the Niger basin experiences average annual rainfall

227 of 700 mm. The spatial rainfall distribution shows north-to-south increasing gradient, with the Sahel region (> 12°N)

228 receiving on average 346 mm per year, the Savanna region (8°N – 12°N) receiving on average 1,206 mm per year,

229 and the Guinea region (4°N – 8°N) receiving on average 1,620 mm per year. The spatial structures (climatology and

230 north-south gradient in rainfall) of GFS, IMERG and CHIRPS rainfall fields are quite similar to those of IMERG

231 Final. However, the 1-day GFS tends to overestimate in the wet Guinea region of the basin, whereas both IMERG

232 Early and CHIRPS give values that are very close to IMERG Final.
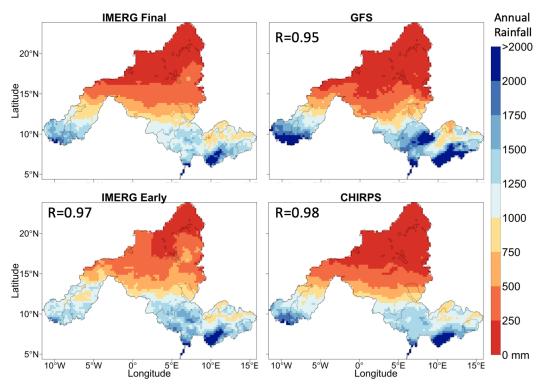
233

234
235 Figure 2. Spatial map of annual rainfall (in mm), for the period 15 June 2019 to 15 June 2020, derived from (a) IMERG Final, (b) GFS (1-day lead time), (c) IMERG Early, and (d) CHIRPS.

Hydrology and
Earth System
Sciences
Discussions

Open Access

EGU

236 Figure 3 shows the seasonal rainfall pattern for each climatological region. According to the reference IMERG Final,

237 as one goes from north to south, the rainy season expands from 3 months (June – September) in the Sahel to 6 months

238 (March – November) in the Savanna and Guinea regions. The peak rainfall also shows north-south gradient, with peak

239 rainfall of 130 mm in the Sahel, to 269 mm in the Savanna, and 350 mm in the Guinea. The rainfall pattern is unimodal

240 with a peak rainfall value in August for both Sahel and Savanna, but becomes bimodal with one peak in May and the

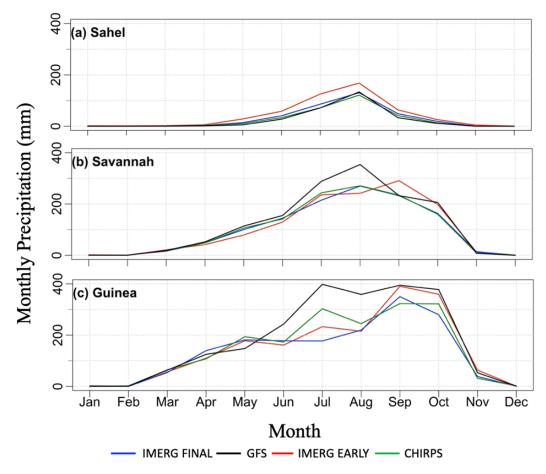241 other in September for Guinea.

242

243 Figure 3. Monthly precipitation regime for the three climatological zones of the Niger river Basin: (a)
244 Sahel, (b) Savanna, and (c) Guinea. Analyses are based on rainfall fields derived from IMERG Final, 1-
     day-lead GFS. IMERG Early, and CHIRPS.

245

246   When validated against IMERG Final, the 1-day lead GFS's performance in capturing the seasonal rainfall

247   characteristics deteriorates as one goes from north to south. GFS captures both the seasonal rainfall pattern and rainfall

248   peak in the Sahel, captures the seasonal rainfall pattern but tends to moderately overestimate the peak in the Savannah,

249   and results in large overestimation (almost twice as much as the reference) in the summer in the Guinea. As far as the

250   other satellite products are concerned, IMERG Early tends to slightly overestimate in the Sahel across all rainy months,

251   but performs relatively well in the Savannah and Guinea regions. CHIRPS is very close to IMERG Final in all regions

252   and months, with the exception of modest overestimation of the July rainfall in Guinea.

253   **3.2 How well is the annual precipitation total forecasted in each dam watershed?**

254   Figure 4 presents the watershed-averaged annual rainfall (15 June 2019 – 15 June 2020) for each dam watershed.

255   According to IMERG Final, annual rainfall varies from 434 mm (in Kainji) to 1,481 mm (in Selingue). Watersheds 1

256   (Selingue) and 2 (Markala), located in the western part of the Savannah, receive the largest amount of rainfall, i.e.,

257   1481 mm and 1406 mm, respectively. Watershed 3 (Markala), located in the eastern part of the Sahel, receives 741

258   mm of annual rainfall. Watershed 4 (Bakolori), characterized by the smallest watershed area compared to the rest of

259   the watersheds, lies partly in the Sahel and partly in the Savannah region and receives 921 mm of annual rainfall.

260   Watershed 5 (Kainji), characterized by the largest watershed area of all, lies mostly in the Sahel region and receives

261   the lowest amount of annual rainfall (434 mm). Watersheds 6 (Jebba), 7 (Dadin Kowa), and 8 (Lagdo), located in the

262   Savannah, receive annual rainfall amounts of 1190 mm, 941 mm, and 1295 mm, respectively.

263

264   Validated against IMERG Final, the GFS tends to overestimate rainfall in all watersheds located in the Savannah (or

265   watersheds that receive relatively large rainfall amounts), with an overestimation varying in the range 8% to 33%,

266   with larger bias for watersheds receiving higher rainfall amount. For watersheds in the Sahel (watersheds receiving

267   low rainfall amount), GFS gives less bias (-11% for the driest Kainji watershed and +10% for Bakolori).

268

269   In contrast, IMERG Early tends to underestimate rainfall in all watersheds located in the Savannah, with larger

270   negative bias in watersheds with large rainfall amount, but tends to overestimate in all watersheds located in the Sahel

271   with very large overestimation bias for the driest watershed (+48% for Kainji). Therefore, GFS and IMERG Early

272   have different bias characteristics. Whereas GFS outperforms IMERG Early in the Sahelian climate where well-

273   organized convective systems dominate the monsoon, IMERG Early outperforms GFS in the Savannah and Guinea

274   climate which are characterized by short-lasting and localized systems and wet land surface conditions. CHIRPS

275   estimates are reasonably close to IMERG Final, indicating that the choice of reference product between CHIRPS and

276   IMERG Final would not substantially affect the findings on the accuracy of GFS forecasts.
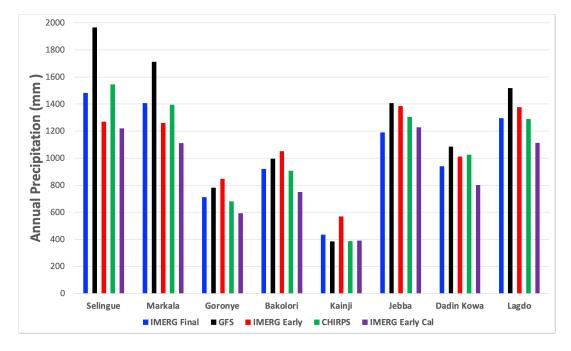
277

278

Figure 4. Sub-basin averaged annual precipitation (mm) for the period, 15 June 2019 to 15 June 2020, for each
of the Niger's sub-basin, derived from the 1-day lead GFS forecast and different satellite precipitation
products.

282

283   **3.3 How well is the time series of daily precipitation forecasted?**

284   Figures 5 and 6 present the time series of watershed-averaged daily rainfall, for the wet period June – October.

285   According to IMERG Final, the temporal variability (as measured through coefficient of variation or CV) varies from

286   1.22 to 2.60. Validated against IMERG Final, the GFS tends to underestimate the temporal variability and particularly

287   underestimate large spikes in rainfall, at almost all sites except at Kainji. The GFS' better performance for Kainji

288   could be attributed to the watershed's large area that results in relatively smooth temporal variability. Both IMERG

289   Early and CHIRPS provide CV values that are very close to those of IMERG Final.
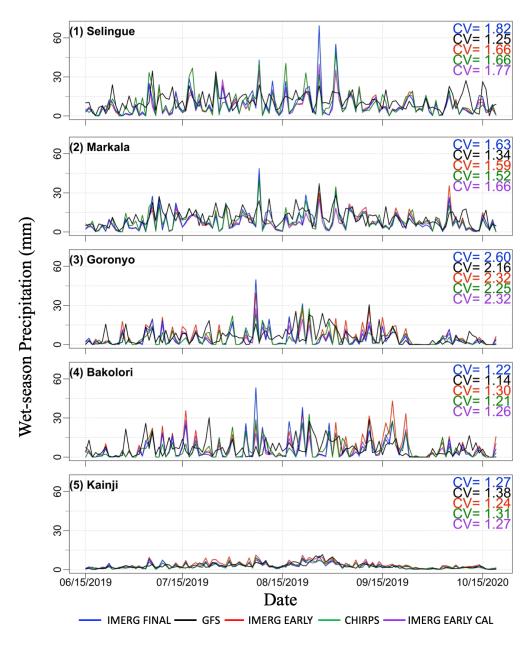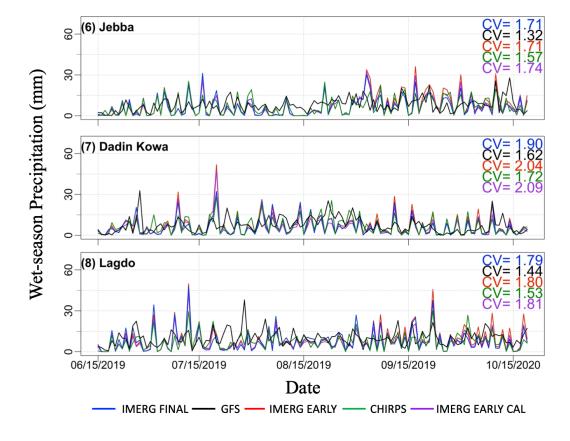
290

Figure 5. Time series of sub-basin averaged precipitation total (mm) for the wet period (June –
September 2019 for all sub-basins, derived from various precipitation products, for five sub-basins.
The Figure also shows the coefficient of variation (CV) as a measure of temporal variation.

291

292

293

Figure 6. Same as in Figure 5 but for the remaining three watersheds.

294

295

296

297

298

299

300

301

302

303

304   Figure 7 displays the performance statistics of watershed-averaged daily rainfall (validated against IMERG Final) in

305   terms of Kling-Gupta Efficiency (KGE), Bias Ratio (BR), correlation (R), variability ratio (γ), and root mean square

306   error normalized by reference precipitation mean (NRMSE). First, the performance results for the 1-day lead GFS

307   were considered. The KGE scores are poor (0.3 < KGE < 0.5) for half of the watersheds considered (Selingue, Goronyo,

308   Bakolori, and Lagdo) and intermediate (0.5 < KGE < 0.75) for the remaining half (Markala, Kainji, Jebba, and Dadin

309   Kowa). The breakdown of the KGE scores (BR, R, and γ) reveals the key factors contributing to the KGE estimates.

310   The GFS tends to overestimate daily precipitation for most sub-basins, as BR is higher than one, except for Kainji.

311   The overestimation is particularly high for Selingue and Markala, where BR is 1.33 and 1.22, respectively. The

312   correlation coefficient between GFS and IMERG Final is mostly low (R < 0.60), and is particularly lower for Bakolori

313   (R=0.36) an Goronyo (R=0.43). The variability ratio of GFS is mostly between 0.69 to 0.83 (except for Kainji, where

314   γ is 1.09), indicating that the GFS tends to give lower temporal variability of rainfall. The NRMSE is very high,

315   ranging from 100% to 266%, and is particularly high for Goronyo (266%) and Bakolori (264%), which are relatively

316   small-sized watersheds.

317

318   Next, the performance of IMERG Early was examined with respect to IMERG Final, mainly to assess if it is possible

319   to use the near-real-time IMERG Early product to calibrate and improve the accuracy of GFS forecasts. The IMERG

320   Early performs much better with KGE values higher than 0.75 (except for Kainji where KGE is 0.69), correlation

321   higher than 0.90, and variability ratio close to the optimum value. The high performance of IMERG Early is due to its

322   similarity with the IMERG Final product, and the main difference between the two products is that IMERG Early,

323   unlike IMERG Final, does not use monthly rain gauge observations for bias correction. Such monthly-based bias

324   corrected procedures would not alter the temporal pattern of IMERG Early as compared that of IMERG Final. In terms

325   of bias, IMERG Early slightly underestimates rainfall in the Selingue and Markala watersheds (by 14% and 11%,

326   respectively), where GFS has large overestimation bias (by 33% and 22%, respectively), but overestimates rainfall in

327   the rest of the watersheds in the range 6% to 31%. The overestimation is particularly high for Kainji (31%), where

328   GFS has lower bias at -12%. Therefore, there is no winner between GFS and IMERG Early as far as bias is considered.

329

330 CHIRPS was also compared with IMERG Final to assess how the use of different reference products may affect the

331 finding about the performance of GFS forecasts. The KGE scores of CHIRPS are higher than 0.75 in all cases,

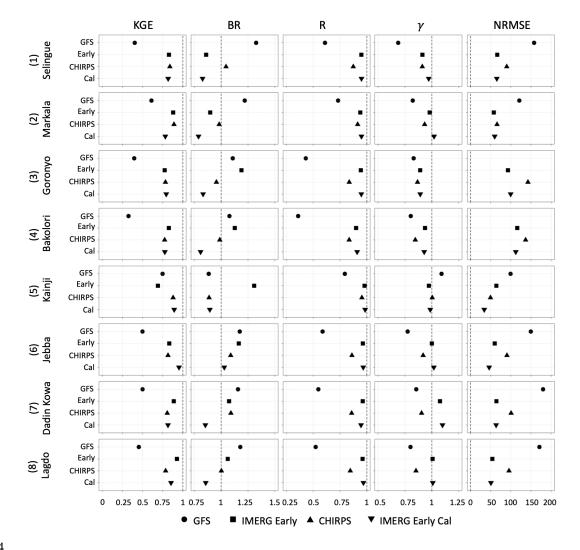332 indicating that CHIRPS and IMERG Final have comparable KGE performance.

333

334
335 Figure 7. Summary of performance statistics (Kling-Gupta Efficiency KGE, Bias Ratio BR, correlation R, variability ratio γ, and root mean square error normalized by reference rainfall [%], for the 1-day lead time GFS forecasts and other satellite products.
336
337

338   **3.4 Dependence of Forecast Uncertainty on Precipitation Rate**

339   Figure 8 compares pairs of 1-day lead GFS forecasts and IMERG Final, for daily and watershed-average scales. The

340   performance of GFS varies between watersheds. In the Markala and Kainji watersheds, GFS forecasts agree well

341   with IMERG Final at almost all rain rates. In the Selingue watershed, GFS agrees well with IMERG Final for rain

342   rates under 30 mm/day, but GFS substantially underestimates all rain rates above 30 mm/day. In the remaining five

343   watersheds, GFS has poor performance, replete with large scatter, high false alarm, and large underestimation bias
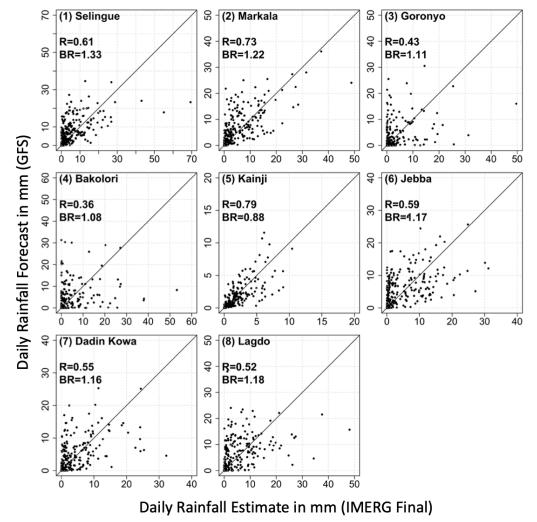
344   of heavy rain rates.

Figure 8. Scatterplot of watershed-averaged daily precipitation forecast obtained from 1-day lead GFS
forecasts against corresponding values from IMERG Final.

345

Hydrology and
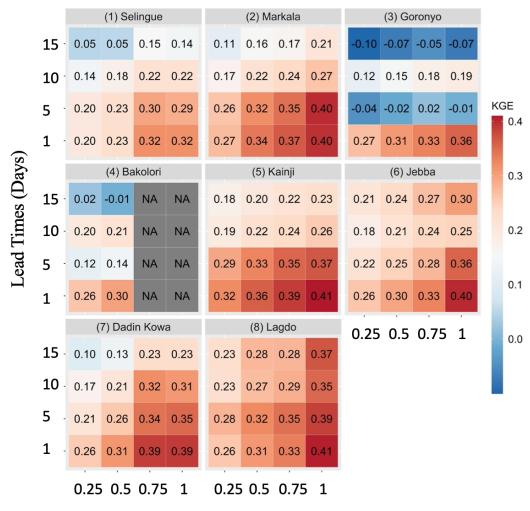Earth System
Sciences
Discussions
Open Access
EGU

346   **3.5 Performance of climatological bias correction of IMERG Early**

347   As discussed above, IMERG Early estimates are biased, and in some cases, the biases are worse compared to those of

348   GFS. One approach to improve the performance of IMERG Early may be to remove the bias through climatological

349   bias correction. Climatological bias correction of the IMERG Early estimates was performed by calculating the bias

350   ratio between the long-term average (2001-2018) IMERG Final and IMERG Early estimates at each pixel for each

351   month, and multiplying the IMERG Early estimates during the study period (15 June 2019 – 15 June 2020) by the

352   monthly bias ratio at each pixel.

353

354   The performance of the climatologically-bias-corrected IMERG Early estimates (referred to as "IMERG Early Cal")

355   is shown in Figures 4 – 7 and Figure 11. The IMERG Early Cal estimates have still large biases, and in some cases,

356   these biases are worse than the raw IMERG Early estimates (see Figs. 7 and 11). In five watersheds (Selingue, Markala,

357   Bakolori, Dadin Kowa and Lagdo), the raw IMERG Early have better KGE compared to IMERG Early Cal, whereas

358   the reverse is true in the remaining three watersheds. Therefore, such climatological bias correction approach is not

359   effective in removing the bias in IMERG Early estimates, and indicates the need to explore other bias correction

360   strategies.

361

362   **3.6 Dependence of Daily Forecast Uncertainty on Lead Time and Spatial Scale**

363   Figure 9 shows the performance of daily GFS forecasts for different grid sizes (0.25°, 0.5°, 0.75°, and 1°) and lead

364   times (1-day, 5-day, 10-day, and 15-day), in terms of KGE. Increasing spatial scale for a given watershed increases

365   KGE. For example, in the Markala watershed, the KGE increases from 0.27 (at 0.25°) to 0.40 (at 1.0°), for a 1-day

366   lead. Increasing the lead time of forecasts decreases the KGE value of daily rainfall. For example, for the Markala

367   watershed and a grid size of 1°, the KGE for daily rainfall forecast was decreased from 0.40 (1-day lead) to 0.21 (15-

368   day lead).

369

370   The variation in KGE values between the watersheds could be partly explained by the watershed size. For example,

371   based on Fig. 5, the KGE for the 1-day lead daily GFS forecast was the highest for the largest Kainji watershed

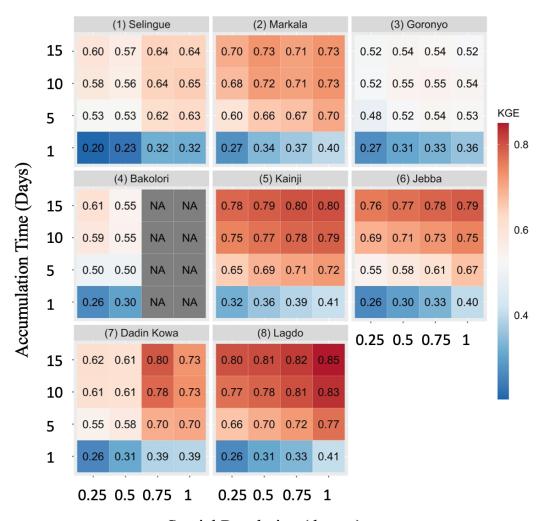372   (watershed area of 1,464,092 sq. km) and the lowest for the smallest Bakolori watershed (4,887 Sq. km).

373

374
375
376
377
378

379
380 Figure 9. Kling-Gupta Efficiency (KGE) for daily precipitation of GFS as a function of lead time (1-
day, 5-day, 10-day, and 15-day) and spatial scale (0.25°, 0.50°, 0.75°, 1.0°).

381

382

383

Hydrology and
Earth System
Sciences
Discussions

384

385
386
Figure 10. Kling-Gupta Efficiency (KGE) of GFS as a function of accumulation time scale (1-day, 5-
387 day, 10-day, and 15-day) and spatial scale (0.25°, 0.50°, 0.75°, 1.0°).

388

389

390

391

392 **3.7 Effect of Temporal Aggregation Scale on Forecast Uncertainty**

393 To assess the effect of temporal aggregation scale, we obtained the 1-day total, 5-day total, 10-day total, and 15-day

394 total GFS precipitation forecasts were calculated. These multi-day forecasts are constructed by combining multiple

395 lead-time forecasts. For instance, the 5-day total forecast is obtained by adding the 1-day lead, 2-day lead, 3-day lead,

396 4-day lead, and 5-day lead daily forecasts. Figure 10 presents the KGE values for GFS forecasts over different

397 temporal aggregation scales, and different grid sizes. Temporal aggregation substantially increases KGE at all spatial

398 scales. For example, in the Markala watershed and the grid size of 1°, the KGE values jump from 0.40 at daily

399 timescale to 0.73 at 15-day total timescale.

400

401 In Figure 11, the performance statistics of GFS for 15-day accumulated rainfall forecast averaged over each watershed

402 are shown. The KGE values are intermediate ($0.5 < KGE < 0.75$) for four watersheds and good ($KGE > 0.75$) for the

403 remaining four watersheds. Analysis of the components of KGE reveals that the improvement of KGE at longer

404 timescales comes as a result of improved correlation and variability ratio. At the 15-day accumulation timescale,

405 IMERG Early estimates have less bias than GFS at all watersheds, except for the Kainji watershed. The IMERG Early

406 Cal estimates have not shown significant improvements over IMERG Early at most watersheds, except for Kainji and

407 Jebba watersheds. Figure 12 presents the scatterplot of 15-day accumulated GFS forecast vs IMERG Final. The

408 performance of GFS varies with rain rates. In general, the GFS estimates perform well for low to moderate rain rates,
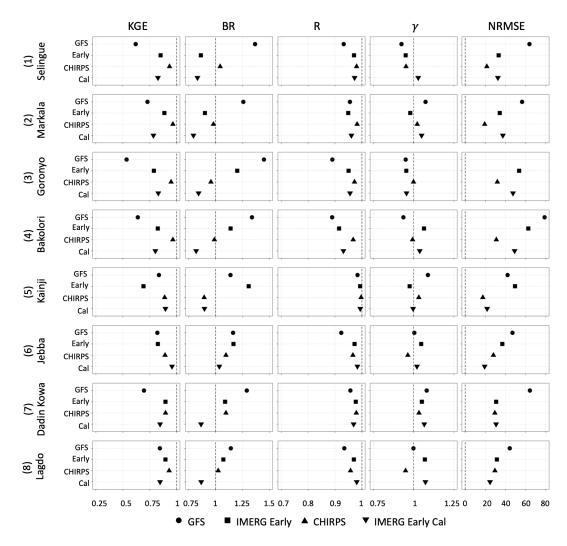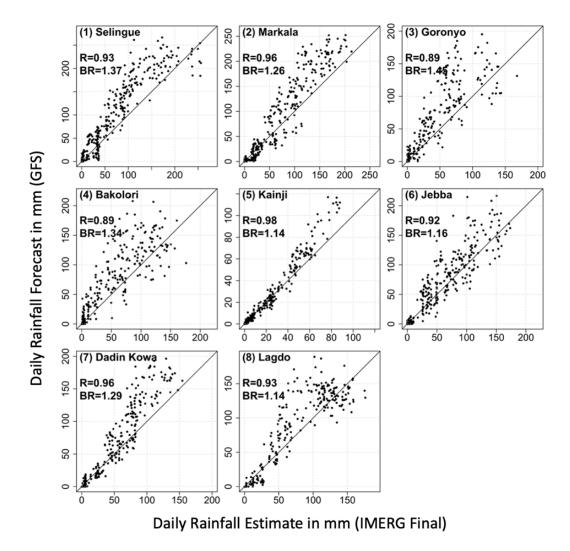
409 but tend to overestimate higher rain rates.

410

411

412

413

414

415

416

417

Figure 11. Summary of performance statistics (Kling-Gupta Efficiency KGE, Bias Ratio BR, correlation R, variability ratio γ, and root mean square error normalized by reference rainfall [%], for the 15-day accumulated GFS forecast and other satellite products.

420

421
422
423   Figure 12. Scatterplot of watershed-averaged 15-day accumulated precipitation forecast obtained from GFS
       forecast against corresponding values from IMERG Final.

424

425

426

427

428

429   **4.   Conclusions**

430   This study has evaluated the accuracy of medium-range (1-day to 15-day lead time) forecasts available from the

431   Global Forecast System (GFS), for the watersheds of large dams in the Niger river basin. Despite the limited

432   temporal coverage, some consistent featured emerged from this evaluation. The accuracy of GFS forecast depends

433   on lead time, accumulation timescale, spatial scale, and climatological regime. At the daily timescale, the

434   performance of GFS forecasts is low for most watersheds. The only two watersheds where the GFS forecasts are

435   reasonable are Markala and Kainji, both of which have larger watershed area compared to the rest of the watersheds.

436   The GFS forecast accuracy drastically increases at longer accumulation timescales. At the 15-day accumulation

437   timescale, the KGE values are either intermediate (Selingue, Goronyo, Bakolori, and Daddin Kowa) or good

438   (Markaa, Kainji, Jebba, and Lagdo). The increase in KGE with increasing accumulation time scale comes as a result

439   of improved correlation between forecasts and IMERG Final. The GFS bias varies with rain rate; the GFS forecasts

440   are almost unbiased at low to medium rain rates, but have large overestimation bias at high rain rates.

441

442   The GFS forecast has large overestimation bias in the Guinea (wet climatic regime), moderate overestimation bias in

443   the Savannah (moderately wet climatic regime), but has no bias in the Sahel (dry climate). Whereas GFS

444   outperforms IMERG Early in the Sahelian climate where well-organized convective systems dominate the monsoon,

445   IMERG Early outperforms GFS in the Savannah and Guinea climate which are characterized by short-lasting and

446   localized systems and wet land surface conditions. For a given climatic regime, the larger the watershed, the higher

447   is the accuracy of GFS in terms of KGE.

448

449   The study has further examined the potential of the near-real-time product IMERG Early to calibrate and further

450   improve the accuracy of GFS forecasts. The KGE values for IMERG Early are overall greater than those for GFS,

451   indicating that calibration of GFS based on IMERG Early can lead to increases in KGE mainly due to improvements

452   in correlation and variability ratio. However, in terms of bias, there is no clear winner between GFS and IMERG Early

453   at the daily time scale. As the timescale increases, IMERG Early starts outperforming GFS in bias. Climatological

454   bias correction of IMERG Early, through comparison of the long-term average of IMERG Final and IMERG Early,

455   is not effective in removing the bias in IMERG Early estimates.

456

457 Overall, we conclude that the GFS forecast, at 15-day accumulation timescale, has acceptable performance in terms

458 of KGE, however, the forecasts are highly biased particularly at high rain rates. It is recommended to apply bias

459 correction of GFS forecasts in order to effectively use them in applications. The use of IMERG Early to calibrate GFS

460 would improve GFS in terms of correlation and variability, but not in terms of bias. Climatological bias correction of

461 IMERG Early is not found to be effective in reducing the bias in IMERG Early. It is recommended to identify robust

462 bias correction methods appropriate for IMERG Early.

463

464

465

466

467

468

469

470

471

472

473

474

475

476

477

478

479

480

481

482

483

484 **5. Data and Code Availability**

485   We acknowledge the National Center for Atmospheric Research (NCAR) for providing public access to the GFS

486   rainfall forecast data products (https://rda.ucar.edu/datasets/ds084.1/), NASA for providing public access to IMERG

487   Final and IMERG Early rainfall data products (https://disc.gsfc.nasa.gov), and the University of California Santa

488   Barbara's (UCSB) Climate Hazard's group for providing public access to CHIRPS rainfall data

489   (https://www.chc.ucsb.edu/data).

490

491

492   **6. Author Contribution**

493   H. Yue: data processing, data analysis, and manuscript preparation; M. Gebremichael: project oversight, method

494   design, contribution to manuscript text; V. Nourani: method design, contribution to manuscript text.

495

496

497   **7. Competing Interests**

498   The authors declare that they have no conflict of interest.

499

500

501   **8. Acknowledgement**

503

References

504 **References**

506 Abdalla, S., Janssen, P. A., Balmaseda, M. A., Mogensen, K., Bidlot, J. R., & Keeley, S.: ECMWF Experience In
507 Global Monitoring And Validation Of Radar Altimetry Products. In ESA Living Planet Symposium 2013, 9-13 Sep.
508 2013, Edinburgh, ESA Proceedings No. SP-722 (CD), 2013 December

509 Akinsanola, A.A., Ajayi, V.O., Adejare, A.T., Adeyeri, O.E., Gbode, I.E., Ogunjobi, K.O., Nikulin, G. and Abolude,
510 A.T.: Evaluation of rainfall simulations over West Africa in dynamically downscaled CMIP5 global circulation
511 models. Theoretical and applied climatology., 132(1), 437-450, doi:10.1007/s00704-017-2087-8, 2017.

512 Akinsanola, A. A., Ogunjobi, K. O., Gbode, I. E., and Ajayi, V. O.: Assessing the capabilities of three regional climate
513 models over CORDEX Africa in simulating West African summer monsoon precipitation. Advances in Meteorology,
514 doi:10.1155/2015/935431, 2015.

515 Akinsanola, A. A., and Zhou, W.: Projections of West African summer monsoon rainfall extremes from two CORDEX
516 models. Climate Dynamics, 52(3), 2017-2028, doi:10.1007/s00382-018-4238-8, 2018

517 Alexander, S., Yang, G., Addisu, G., and Block, P.: Forecast-informed reservoir operations to guide hydropower and
518 agriculture allocations in the Blue Nile basin, Ethiopia. International Journal of Water Resources Development, 1-26,
519 doi:10.1080/07900627.2020.1745159, 2020

520 Alfieri, L., Burek, P., Dutra, E., Krzeminski, B., Muraro, D., Thielen, J., and Pappenberger, F.: GloFAS–global
521 ensemble streamflow forecasting and flood early warning. Hydrology and Earth System Sciences, 17(3), 1161-1175,
522 doi:10.5194/hess-17-1161-2013, 2013

523 Animashaun, I. M., Oguntunde, P. G., Akinwumiju, A. S., and Olubanjo, O. O.: Rainfall Analysis over the Niger
524 Central Hydrological Area, Nigeria: Variability, Trend, and Change point detection. Scientific African, 8, e00419,
525 doi: 10.1016/j.sciaf.2020.e00419, 2020

526 Arakawa, A., and Schubert, W. H.: Interaction of a cumulus cloud ensemble with the large-scale environment, Part I.
527 Journal of the Atmospheric Sciences, 31(3), 674-701, doi:10.1175/1520-0469(1974)031<0674:IOACCE>2.0.CO;2,
528 1974

529 Bhuiyan, M.A., Nikolopoulos. E.I., and Anagnostou, E.N.: Machine Learning-Based Blending of Satellite and
530 Reanalysis Precipitation Datasets: A Multiregional Tropical Complex Terrain Evaluation, Journal of
531 Hydrometeorology, 20(11), 2147-2161, doi: 10.1175/JHM-D-19-0073.1, 2019.

532 Bliefernicht, J., Waongo, M., Salack, S., Seidel, J., Laux, P., and Kunstmann, H.: Quality and value of seasonal
533 precipitation forecasts issued by the West African regional climate outlook forum. Journal of Applied Meteorology
534 and Climatology, 58(3), 621-642, doi:10.1175/JAMC-D-18-0066.1, 2019.

535 Breuer, N. E., Fraisse, C.W., and Cabrera, V.E.: The Cooperative Extension Service as a boundary organization for
536 diffusion of climate forecasts: A 5-year study. Journal of Extension 48(4), 2010.

537 Chen, F., Janjić, Z., and Mitchell, K. Impact of atmospheric surface-layer parameterizations in the new land-surface
538 scheme of the NCEP mesoscale Eta model. Boundary-Layer Meteorology, 85(3), 391-421, doi:
539 10.1023/A:1000531001463, 1997.

540 Clough, S., Shephard, M., Mlawer, E., Delamere, J., Iacono, M., Cady-Pereira, K., Boukabara, S., and Brown, P.:
541 Atmospheric radiative transfer MODELING: A summary of the AER codes. Journal of Quantitative Spectroscopy
542 and Radiative Transfer, 91(2), 233-244. doi:10.1016/j.jqsrt.2004.05.058, 2005.

543 Dembélé, M., Schaefli, B., van de Giesen, N., and Mariéthoz, G.: Suitability of 17 rainfall and temperature gridded
544 datasets for largescale hydrological modelling in West Africa. Hydrol. Earth Syst. Sci. Discuss., https://doi.
545 org/10.5194/hess-2020-68, in review, 2020

546 Dezfuli, A. K., Ichoku, C. M., Huffman, G. J., Mohr, K. I., Selker, J. S., Van De Giesen, N., Hochreutener, R., and
547 Annor, F. O.: Validation of IMERG precipitation in Africa. Journal of hydrometeorology, 18(10), 2817-2825, doi:
548 10.1175/JHM-D-17-0139.1, 2017

549 Funk, C., Peterson, P., Landsfeld, M., Pedreros, D., Verdin, J., Shukla, S., Husak, G., Rowland, J., Harrison, L., Hoell,
550 A., and Michaelsen, J.: The climate hazards infrared precipitation with stations—a new environmental record for
551 monitoring extremes. Scientific data, 2(1), 1-21, doi:10.1038/sdata.2015.66, 2015.

552 Gossett, M., Alcoba, M., Roca, R., Cloche, S., and Urbani, G.: Evaluation of TAPEER daily estimates and other GPM-
553 era products against dense gauge networks in West Africa, analysing ground reference uncertainty. 144(1), 255-269,
554 doi: 10.1002/qj.3335, 2018.

555 Grell, G. A.: Prognostic evaluation of assumptions used by cumulus parameterizations. Monthly weather review,
556 121(3), 764-787, doi: 10.1175/1520-0493(1993)121<0764:PEOAUB>2.0.CO;2, 1993.

557 Gupta, H. V., Kling, H., Yilmaz, K. K., and Martinez, G. F.: Decomposition of the mean squared error and NSE
558 performance criteria: Implications for improving hydrological modelling. Journal of hydrology, 377(1-2), 80-91, doi:
559 10.1016/j.jhydrol.2009.08.003, 2009.

560 Haile, A. T., Tefera, F. T., and Rientjes, T.: Flood forecasting in Niger-Benue basin using satellite and quantitative
561 precipitation forecast data. International journal of applied earth observation and geoinformation, 52, 475-484, doi:
562 10.1016/j.jag.2016.06.021, 2016.

563 Hou, A. Y., Kakar, R. K., Neeck, S., Azarbarzin, A. A., Kummerow, C. D., Kojima, M., Oki, R., Nakamura, K., and
564 Iguchi, T.: The global precipitation measurement mission. Bulletin of the American Meteorological Society, 95(5),
565 701-722, doi:10.1175/BAMS-D-13-00164.1, 2014.

566 Huffman, G. J., Bolvin, D. T., Nelkin, E. J., Wolff, D. B., Adler, R. F., Gu, G., Hong, Y., Bowman, K.P. and Stocker,
567 E. F.: The TRMM Multisatellite Precipitation Analysis (TMPA): Quasi-Global, Multiyear, Combined-Sensor
568 Precipitation estimates at fine scales. Journal of Hydrometeorology, 8(1), 38-55. doi:10.1175/jhm560.1, 2007.

569 Huffman, G. J., Bolvin, D. T., Braithwaite, D., Hsu, K., Joyce, R., Xie, P., & Yoo, S. H.: NASA global precipitation
570 measurement (GPM) integrated multi-satellite retrievals for GPM (IMERG). Algorithm Theoretical Basis Document
571 (ATBD) Version, 4, 26, 2015.

572 Huffman, G.J., Stocker, E.F., Bolvin, D.T., Nelkin, E.J., Jackson J.: GPM IMERG Final Precipitation L3 1 day 0.1
573 degree x 0.1 degree V06, Edited by Andrey Savtchenko, Greenbelt, MD, Goddard Earth Sciences Data and
574 Information Services Center (GES DISC), Accessed: [Feb 11, 2021], doi:10.5067/GPM/IMERGDF/DAY/06, 2019a

575 Huffman, G.J., Stocker, E.F., Bolvin, D.T., Nelkin, E.J., Jackson J.: GPM IMERG Early Precipitation L3 1 day 0.1
576 degree x 0.1 degree V06, Edited by Andrey Savtchenko, Greenbelt, MD, Goddard Earth Sciences Data and
577 Information Services Center (GES DISC), Accessed: [Feb 11, 2021], doi:10.5067/GPM/IMERGDE/DAY/06, 2019b

578 Iacono, M. J., Mlawer, E. J., Clough, S. A., and Morcrette, J. J.: Impact of an improved longwave radiation model,
579 RRTM, on the energy budget and thermodynamic properties of the NCAR community climate model, CCM3. Journal
580 of Geophysical Research: Atmospheres, 105(D11), 14873-14890, doi: 10.1029/2000JD900091, 2000.

581 JMA.: Outline of the operational numerical weather prediction at the Japan Meteorological Agency (Appendix to
582 WMO numerical weather prediction progress report). Japan Meteorological Agency, 47pp. (available online
583 at https://www.jma.go.jp/jma/jma-eng/jma-center/nwp/outline2019-nwp/index.htm; last accessed: February 2021),
584 2019.

585 Kling, H., Fuchs, M., and Paulin, M.: Runoff conditions in the upper Danube basin under an ensemble of climate
586 change scenarios. Journal of Hydrology, 424, 264-277, 2012.

587 Koppa, A., Gebremichael, M., Zambon, R.C., Yeh, W.W.G., and Hopson, T.M.: Seasonal Hydropower Planning for
588 Data-Scarce Regions Using Multimodel Ensemble Forecasts, Remote Sensing Data, and Stochastic Programming.
589 WATER RESOURCES RESEARCH, 55(11), 8583-8607, DOI: 10.1029/2019WR025228, 2019.

590 Maranan, M., Fink, A. H., Knippertz, P., Amekudzi, L. K., Atiah, W. A., and Stengel, M.: A process-based validation
591 of GPM IMERG and its sources using a mesoscale rain gauge network in the West African forest zone. Journal of
592 Hydrometeorology, 21(4), 729-749, 2020

593 Mase, A. S., and Prokopy, L.S.: Unrealized Potential: A review of perceptions and use of weather and climate infor-
594 mation in agricultural decision making. Weather Climate and Society 6(1):47-61. DOI: 10.1175/Wcas-D-12-00062.1,
595 2014.

596 Mlawer, E. J., Taubman, S. J., Brown, P. D., Iacono, M. J., and Clough, S. A.: Radiative transfer for inhomogeneous
597 atmospheres: RRTM, a validated correlated-k model for the longwave. Journal of Geophysical Research:
598 Atmospheres, 102(D14), 16663-16682, 1997.

599 National Centers for Environmental Prediction.: National Centers for Environmental Prediction: The Global Forecast
600 System (GFS) -Global Spectral Model (GSM). Retrieved from
601 https://www.emc.ncep.noaa.gov/emc/pages/numerical_forecast_systems/gfs/documentation.php, last access: Sep
602 2020, 2019a

603 National Centers for Environmental Prediction.: National Centers for Environmental Prediction: FV3: The GFDL
604 Finite-Volume Cubed-Sphere Dynamical Core, Retrieved from https://vlab.ncep.noaa.gov/web/fv3gfs, last access:
605 Sep 2020), 2019b

606 National Centers for Environmental Prediction/National Weather Service/NOAA/U.S. Department of Commerce.:
607 NCEP GFS 0.25 Degree Global Forecast Grids Historical Archive, doi:10.5065/D65D8PW, 2015

608 Pandya, R., Hodgson, A., Hayden, M.H., Akweongo, P., Hopson, T., Forgor, A.A., Yoksas, T., Dalaba, M.A., Dukic,
609 V., Mera, R., and Dumont, A., McCormack, K., Anaseba, D., Awine, T., Boehnert, J., Nyaaba, G., Laing, A., and
610 Semazzi, F.: Using weather forecasts to help manage meningitis in the West African Sahel. Bulletin of the American
611 Meteorological Society 96(1):103-+. doi: 10.1175/Bams-D-13-00121.1, 2015

612 Patt, A. G., Ogallo, L., and Hellmuth, M.: Sustainability—Learning from 10 years of climate outlook forums in Africa.
613 Science 318(5847):49-50. doi:10.1126/science.1147909, 2007.

614 Pirret, J. S., Daron, J. D., Bett, P. E., Fournier, N., and Foamouhoue, A. K.: Assessing the skill and reliability of
615 seasonal climate forecasts in Sahelian West Africa. Weather and Forecasting, 35(3), 1035-1050, doi:10.1175/WAF-
616 D-19-0168.1, 2020.

617 Roudier, P., Alhassane, A., Baron, C., Louvet, S., and Sultan, B.: Assessing the benefits of weather and seasonal
618 forecasts to millet growers in Niger. Agricultural and forest meteorology, 223, 168-180, doi:
619 10.1016/j.agrformet.2016.04.010, 2016.

620 Saha, S., Moorthi, S., Wu, X., Wang, J., Nadiga, S., Tripp, P., Behringer, D., Hou, Y.-T., Chuang, H.-Y., Iredell, M.,
621 Ek, M., Meng, J., Yang, R., Mendez, M.P., van den Dool, H., Zhang, Q., Wang, W., Chen, M., and Becker, E.: The
622 NCEP climate forecast system version 2. Journal of climate, 27(6), 2185-2208, doi:10.1175/JCLI-D-12-00823.1,
623 2014.

624 Satgé, F., Defrance, D., Sultan, B., Bonnet, M. P., Seyler, F., Rouché, N., and Paturel, J. E.: Evaluation of 23 gridded
625 precipitation datasets across West Africa. Journal of Hydrology, 581, 124412, doi:10.1016/j.jhydrol.2019.124412 ,
626 2020.

627 Sorí, R., Nieto, R., Drumond, A., and Gimeno, L.: The Niger River Basin Moisture Sources: A Lagrangian
628 Analysis. Atmosphere, 8(2), 38, doi: 10.3390/atmos8020038, 2017.

629 Sylla, M. B., Faye, A., Giorgi, F., Diedhiou, A., and Kunstmann, H.: Projected heat stress under 1.5 C and 2 C global
630 warming scenarios creates unprecedented discomfort for humans in West Africa. Earth's Future, 6(7), 1029-1044, doi:
631 10.1029/2018EF000873, 2018.

632 Tian, D., E. F. Wood, and X. Yuan: CFSv2-based sub-seasonal precipitation and temperature forecast skill over the
633 contiguous United States. Hydrology and Earth System Sciences, 21, 1477–1490, doi:10.5194/hess-21-1477-2017,
634 2017.

635 Yuan, X., E. F. Wood, and M. Liang: Integrating weather and climate prediction: toward seamless hydrologic
636 forecasting. Geophysical Research Letters, 41, 5891–5896, doi:10.1002/2014GL061076, 2914.

637 Zhang, C., Xue, M., Supinie, T. A., Kong, F., Snook, N., Thomas, K. W., Brewster, K., Jung, Y., Harris, L.M. and
638 Lin, S. J.: How well does an FV3-based model predict precipitation at a convection-allowing resolution? Results from
639 CAPS forecasts for the 2018 NOAA hazardous weather test bed with different physics combinations. Geophysical
640 Research Letters, 46(6), 3523-3531, doi:10.1029/2018GL081702, 2019.

641
642